International Journal Of
Industrial Electronics Control and Optimization
Print ISSN: 3517-2645
Online ISSN: 3568-2645
Homepage: https://ieco.usb.ac.ir/

Compact Ultra-Wideband Arch-Shaped Wide-Slot Antenna with High Fidelity Factor and Bandwidth Enhancement for Microwave Imaging of Breast Cancer

Motahareh Arezoomandan[1] | Shahram Mohanna[2] | Ahmad Bakhtiari Shahri[3]

Faculty of Electrical and Computer Engineering, University of Sistan and Baluchestan, Zahedan, Iran.[1,2,3]
Corresponding author's email: mohana@ece.usb.ac.ir

Article Info

Article type:
Research Article

Article history:
Received: 02-August-2024
Received in revised form: 15-October-2024
Accepted: 09-December-2024
Published online: 21-March-2026

Keywords:
Ultra-wideband antenna,
Microwave imaging,
Arch shaped,
Wide-slot,
Fidelity factor.

ABSTRACT

A new compact Ultra-Wide Band (UWB) arch-shaped wide-slot antenna was implemented for Microwave Imaging (MI) of breast cancer. It is composed of a fork-shaped strip and an arched slot ground, with a compact size of 16×20 mm and a height of 1 mm. The arched slot in the ground plate enhances the impedance bandwidth and the gain of the antenna. It has a bandwidth of 3.7 GHz to 18 GHz, covers WLAN (5.4 GHz), X band (8-12 GHz), and Ku band (12-18 GHz), and has a gain of 2.7 dBi to 6.3 dBi in the frequency ranges. The fidelity factor was computed for both E-plane and H-plane scenarios, indicating a range of 0.922 - 0.975 for the E-plane across all angles. It has a small size, a simple design, less signal distortion, a high gain of 6.3 dBi, a fractional bandwidth percentage of 131%, and an efficiency of 93.7% at 6 GHz. It exhibited reliable performance in terms of the fidelity factor at all angles compared to the most recent works. An MI simulation for breast tumor detection was performed to detect changes in the backscattering signal in the presence or absence of a tumor with a high dielectric inclusion. S11 is quite high when measured in front of a breast model. There is a noticeable difference in S21 between the scenarios with and without a tumor in the breast model. There are significant variations in the transmission parameter across the entire frequency range between the scenarios with and without a tumor.

I. Introduction

Microwave Imaging (MI) has the potential for early detection and localization of malignant tissues in the human body [1]. As a non-invasive medical imaging technique, it can be employed to detect breast and brain tumors, image bones, diagnose localized anemia in various parts of the human body, and monitor thermal ablation of liver tumors. Breast cancer is globally recognized as a leading cause of mortality among women [2]. Current imaging techniques for breast cancer detection include X-ray mammography, ultrasound, Magnetic Resonance Imaging (MRI), and combined techniques. Early detection plays a crucial role in successful cancer treatment. The maximum accuracy achieved among these techniques is almost 75.6 percent [3].

MI for breast cancer diagnosis works based on the changes in electrical properties of healthy tissues and tumors. MI is a non-ionizing radiation technique, with proper tissue penetration and low power transmission with fewer health risks [4].

Antennas are essential components of any MI system. Basically, in Ultra-Wide Band (UWB) radar imaging systems, the transmitting antennas emit short UWB pulses and then process the back-scattered signals from the tissue received by the receiving antennas, where significant scattering signatures can be identified and localized. Increasing the bandwidth of these pulses has advantages, including deep tissue penetration at lower frequencies and improved range resolution at higher frequencies. Therefore, the antenna element should possess a

wide bandwidth to transmit such pulses with minimal signal distortion to achieve a high-resolution image of the human body (tissues) [5].

In the microwave radar imaging context, the literature highlights the requirements of using directive antennas with a compact size, very wide frequency bandwidth, high gain and improved efficiency. Specifically for MI of human tissues, it is essential to design antennas that have high-fidelity factors in the time domain [3, 6-9]. Furthermore, the time-domain performance of the antenna must be high to ensure successful penetration through human tissues without significant distortion. Two important distortion characteristics of an antenna are the fidelity factor, which refers to distortion in the time domain, and the group delay, which refers to distortion in the frequency domain [10]. Considering these criteria, UWB antennas are well-suited for MI systems.

Various UWB antennas have been proposed for MI and radar systems, including Vivaldi antennas [11-15], spiral antennas [16], planar monopole antennas [8, 17-19], planar slot antennas [20-22], bowtie antennas, and horn antennas. A comprehensive review of these antennas and their characteristics can be found in [5]. Monopole and wide slot planar antennas are commonly used in antenna arrays for microwave breast imaging systems. These antennas offer advantages such as simple design, small axial length, wide frequency range, and convenient fabrication process. Additionally, designing compact antennas enables more antenna elements to be positioned around the tissue, improving signal utilization and overall resolution [23].

An eagle-shaped UWB patch antenna has also been designed for MI, emphasizing its innovative shape for achieving directional radiation [25]. In comparison with other methods, this work utilizes a simple and effective approach to achieve a bi-directional radiation pattern. In another wide-slot antenna, the radiating element is modified by cutting slots in both patches and the ground plane, enhancing the electrical length to achieve an omnidirectional radiation pattern with a high gain. This method increases the resonance frequency, gain, and efficiency of the antenna without changing its dimensions [20].

In another study [34], the antenna described in [20] has been modified by adding a reflector to create a more directive high-gain antenna. Although this design enhances gain, directivity, and the correlation factor, the large profile of the antenna (29.4 × 32.2 × 25 mm^3) challenges the benefits of compactness and simplicity. In [35], a metamaterial-layer-based lens and an Artificial Magnetic Conductor (AMC) have been utilized to enhance field performance (gain, radiation patterns). Despite achieving high gain, this structure has a larger size (50 × 50 mm^2) and limited impedance matching (2-5 GHz) compared to other designs intended for breast tissue imaging.

Most communication systems prefer to utilize a single radiating element that supports multiple bands and functions, resulting in reduced size and weight [36]. However, for MI, antennas with multi-purpose operation and broader frequency coverage are required. Thus, this project aims to implement an antenna optimized for MI systems. The design of the antenna in this project is based on the structure in [24] exhibiting significant modifications and optimizations to achieve efficient performance in the UWB frequency range.

This project implements a new compact antenna with a high-fidelity factor, which is suitable for MI applications. The antenna has a uniform radiation pattern and notable gain and is efficient in the frequency range, making it suitable for microwave breast imaging applications. The analysis is performed in the time domain, as well as a frequency domain, employing CST Microwave Studio.

II. The Project Overview

The new antenna is composed of a fork-shaped strip, an arched ground slot, and a meander line embedded into the ground plain of the slot. The application of an arched slot in the ground effectively improves both the impedance bandwidth and the gain of the antenna. As a result, the new radiation design provides a wide fractional bandwidth exceeding 131% across its operational range of 3.7–18 GHz. The implementation of novel techniques in designing the antenna's radiation components has led to the attainment of various characteristic parameters, including a maximum simulated gain of 6.3 dBi for the compact antenna. Compared to several documented UWB-based antennas in the literature, the suggested antenna exhibits greater compactness and a wider bandwidth. Moreover, the proposed antenna was analyzed in the time domain was, resulting in a fidelity factor of 0.975 within the frequency range of 3-13 GHz in a face-to-face scenario. This proves a remarkable reduction in signal distortion of the antenna.

An MI simulation for breast tumor detection was performed to detect changes in the backscattering signal in the presence or absence of a tumor with a high dielectric inclusion.

III. Antenna Design

The new wide-slot antenna consists of an arched-shaped slot with meandered arms in a ground plane on one side of an FR4 substrate (with $\varepsilon r = 4.3$ and $\tan \delta = 0.025$). A forked microstrip feed is located on the opposite side of the substrate, as depicted in Fig. 1. The proposed antenna has dimensions of L×W×hs, and a 50Ω coaxial transmission line is used for antenna feeding.

As shown in Figure 2(a), the primary structure has a rectangular slot on its ground plane. In the subsequent stage, an arched-shaped aperture is implemented on the ground plane of the antenna, as depicted in Figure 2(b). This alteration is intended to generate extra resonant frequencies and enhance the return loss. The last step involves using the meandering technique to decrease the lowest operating frequency of the

antenna. Through the implementation of meandering, the current path is extended, resulting in antenna miniaturization and improved matching (lower S11) within the 6-13 GHz range. The proposed antenna is displayed in Fig. 2(c). The parameters for the final antenna configuration, leading to a reflection coefficient (S11) below -10 dB across the frequency range of 3.6-18.5 GHz, can be found in Table I. Figures 3 and 4 show the simulated return loss performance, gain, and efficiency of the designed structure throughout the evolution process.

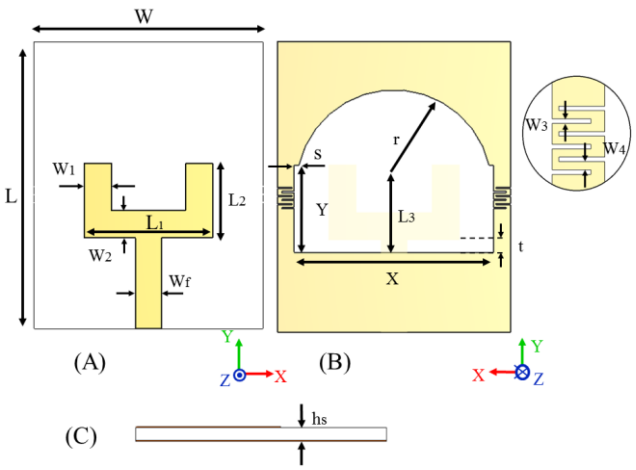

Fig. 1. The geometry of the proposed wide-slot antenna: A) top view, B) bottom view, and C) side view.

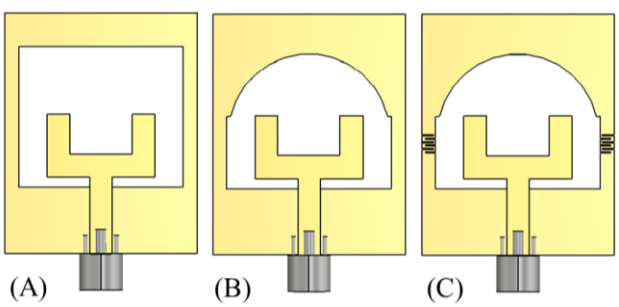

Fig. 2. The structure of the various antennas: A) basic structure, B) basic structure with an arched shape slot, and C) basic structure with arched shape slot and meandered arms (the proposed antenna).

Figure 5 demonstrates the impact of design parameters t, L1, L2, and W3 on S11 by varying one parameter at a time, while keeping all other parameters fixed at the values specified in Table I. This parametric study aimed to investigate the impact of specific antenna design parameters on overall performance. The plot illustrates the relationship between the antenna's reflection coefficient (S11) and each of the four parameters.

Optimal values for these parameters were determined based on achieving the widest bandwidth for S11 below -10 dB (indicated by the black solid line). The substantial influence of all the parameters on the antenna's return loss

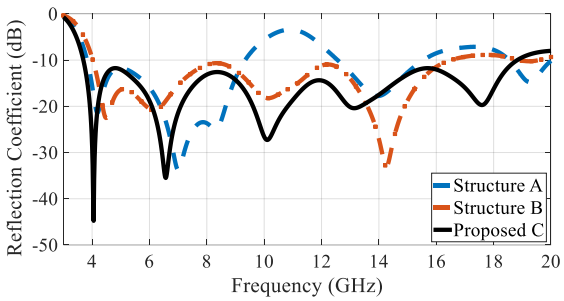

Fig. 3. Simulated reflection coefficient characteristics for various wide-slot antenna structures, as illustrated in Figure 2.

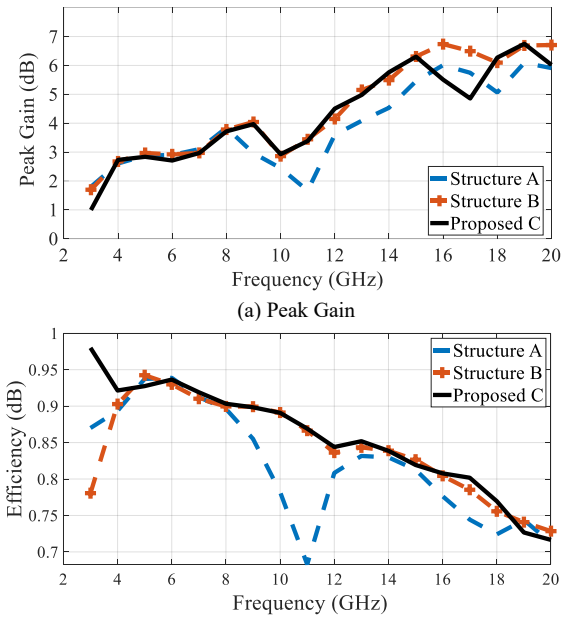

Fig. 4. Simulated (a) gain and (b) efficiency for various wide-slot antenna structures.

is observed through the plots. Changing the distance of t has a significant effect on S11 performance, and when t = 0, the return loss performance deteriorates. As shown in Figure 5(b), the upper frequency of the bandwidth decreases as L1 increases. Additionally, changing the width of W3 can affect both the lower and upper frequencies of the bandwidth.

IV. Frequency Domain Analysis

The fabricated images of the designed wide-slot antenna, including both the front and back views, are illustrated in Figure 6(a). To validate the performance of the antenna, the measured results are compared with the simulated results.

The return loss results obtained from the measurements and simulations in free space demonstrate a satisfactory agreement, as depicted in Figure 6(b). The wide-slot antenna exhibits a measured bandwidth of 10 dB return loss, ranging from 3.7 to 18 GHz.

Figures 7(a) to (c) display the measured and simulated far-field radiation patterns of the wide-slot antenna at frequencies

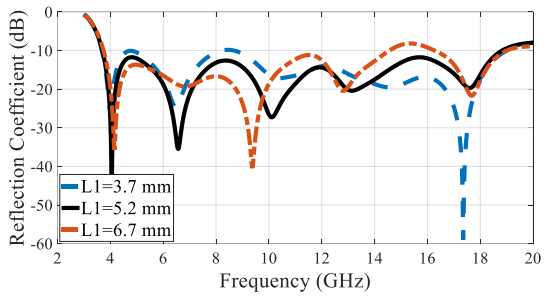

(a) L1

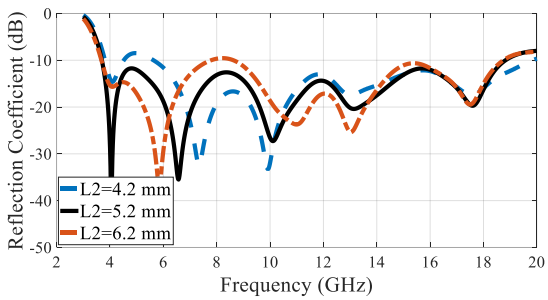

(b) L2

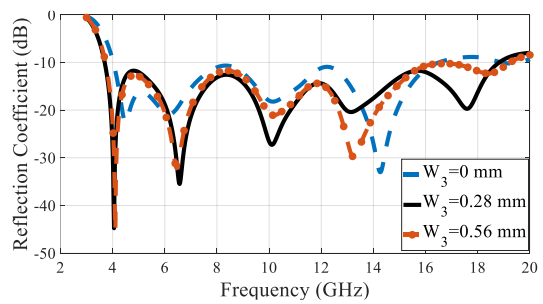

(c) W3

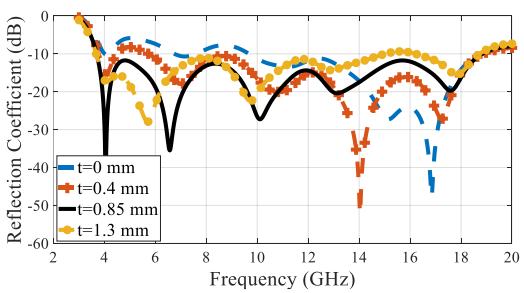

(d) t

Fig. 5. The impact of design parameters t, L1, L2 and W3 on S11 by varying one parameter at a time, with respect to (a) distance t, (b) forked width L1, (c) forked length L2, and (d) meandering width W3. The finalized parameters correspond to the (black) solid line in all plots.

of 4, 8, and 12 GHz. The radiation patterns for the E-plane (y-z plane) and H-plane (x-z plane) are presented, showing a satisfactory alignment between the measured and simulated patterns. This agreement indicates a strong correlation between the predicted and observed radiation characteristics of the antenna.

TABLE 1 PARAMETERS OF THE ANTENNA SHOWN IN FIG.1

Parameter	Value	Parameter	Value
L	20mm	W2	1.9mm
W	16mm	W3	0.1mm
X	13.7mm	W4	0.2mm
Y	6mm	Wf	1.83mm
L1	5.2mm	R	6.7mm
L2	5.2mm	S	0.32mm
L3	4.5mm	T	0.28mm
W1	1.9mm	Hs	1mm

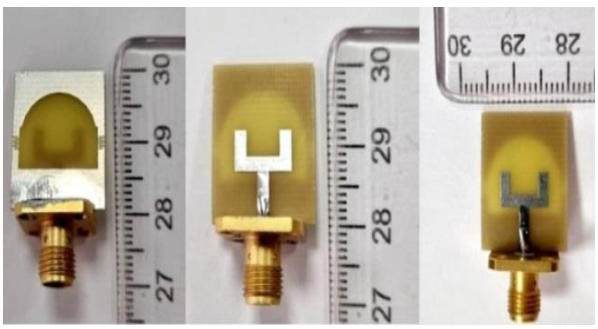

(a) Fabricated Antenna

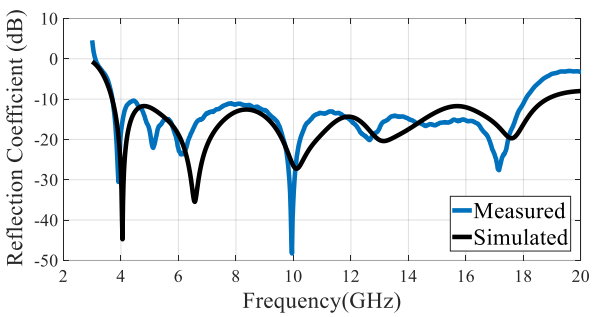

(b) Reflection coefficient

Fig. 6. (a) Photo of fabricated UWB scheme in the front and back view. (b) Measured and Simulated curve of Reflection Coefficient

Figure 8 compares the measured and simulated changes in gain for the proposed antenna. At a frequency of 15 GHz, the simulated and measured gain for the proposed antenna reaches its highest values of 6.3 dBi and 8.6 dBi.

V. Time Domain Analysis

MI systems utilize UWB antennas to transmit data using short pulses across a wide frequency range. However, these narrow pulses are susceptible to dispersion, resulting in distortion upon reception. Nevertheless, the receiver is still capable of recognizing and interpreting the incoming pulse. To mitigate this issue, a time domain analysis of the transmitted pulse is conducted to anticipate and compensate for the system-induced distortion. So, the antenna must have high time-domain performance to effectively penetrate pulses in human tissues and minimize waveform distortions. The fidelity factor is employed to quantify the distortion in the time domain.

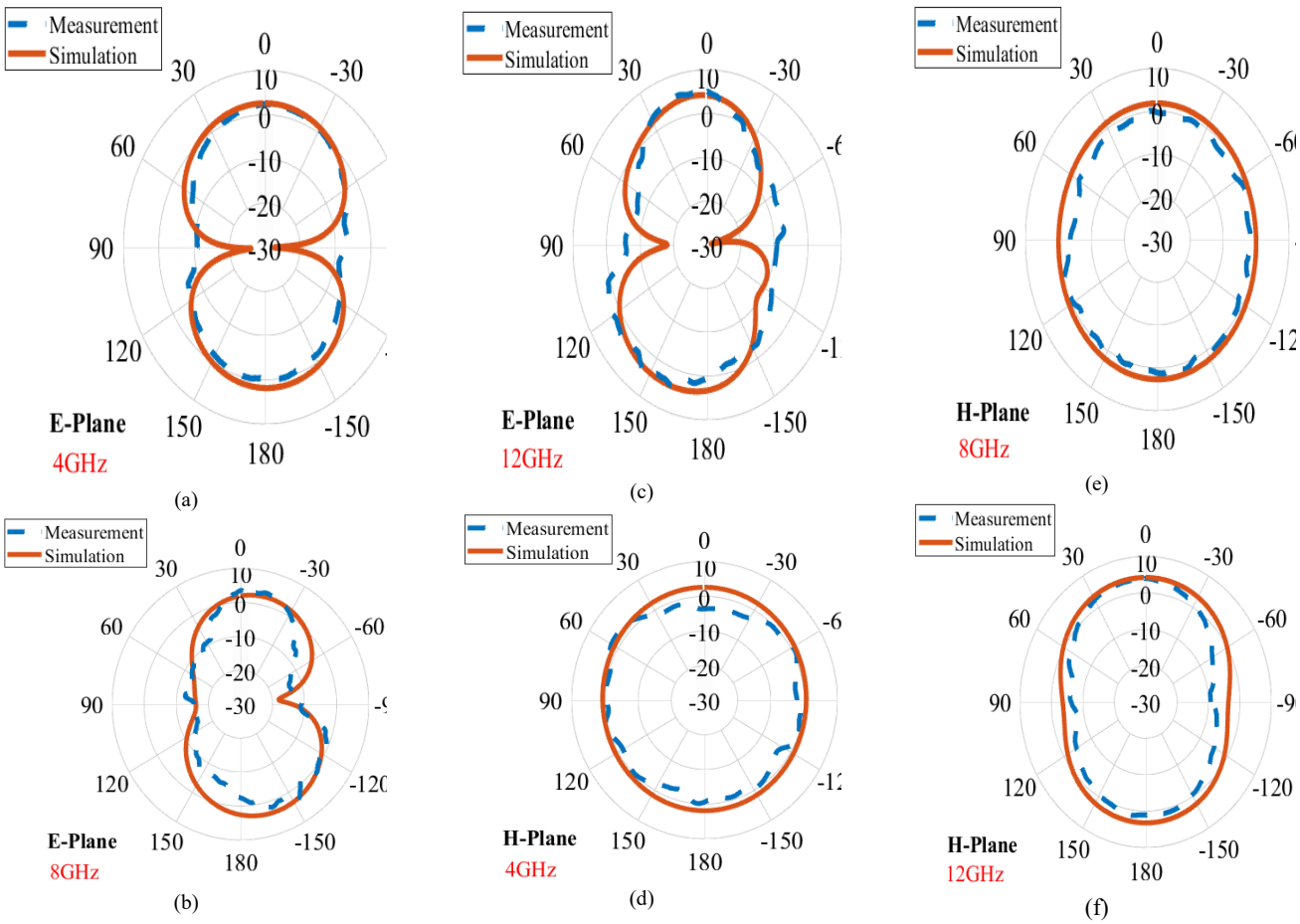

Fig. 7. The simulated and measured radiation patterns at 4 GHz, 8 GHz and 12 GHz. (a-c) E-Plane, (d-f) H-plane.

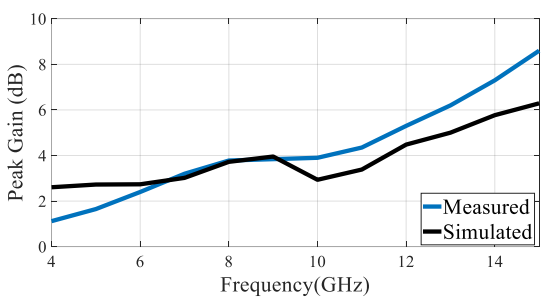

Fig. 8. The simulated and measured gain.

It utilizes the frequency domain transmission coefficient (S21) to compute the correlation between the received and transmitted signals. The fidelity factor depends on various parameters, including the incident signal waveform, gain, and return loss [8]. The calculation of the fidelity factor involves determining the maximum amplitude of the cross-correlation between the received and transmitted signals.

The fidelity factor (FF) is given by:

$$FF = \max_{\tau} \int_{-\infty}^{+\infty} \hat{T}(t)\hat{R}(t+\tau) \quad (1)$$

where $\hat{T}(t)$ and $\hat{R}(t)$ are the normalized transmitted and received signals. To obtain the received signal in the time domain, the following relation can be used:

$$R(\omega) = FFT\big(T(t)\big)H(\omega) \quad (2)$$

$$R(t) = IFFT(R(\omega)) \quad (3)$$

where H(ω) is the system transfer function and is also equivalent to S21, based on the above relationship. To minimize distortion in the received signal in the time domain, the antenna transfer function should possess a flat magnitude.

Group delay is a significant parameter that describes the response of UWB antennas in the frequency domain. It is defined as the derivative of the phase response ∠H(ω) [10].

To ensure minimal signal distortion during pulse transmission, it is necessary for the group delay of the antenna to be constant or have a deviation of less than 1 ns within its operating frequency band. The formula for calculating group delay is:

$$\tau = -\frac{d\phi(\omega)}{d(\omega)} \quad (4)$$

where ϕ represents the phase of the transfer function and ω represents the angular frequency.

Consistency in the magnitude of the antenna transfer function across the operating bandwidth is essential to minimize fluctuations in group delay [8]. This, in turn, is crucial for ensuring limited signal distortion and maintaining a high-fidelity factor in the time domain. Therefore, there is an interconnection between the group delay in the frequency domain and the fidelity factor in the time domain.

To demonstrate it, we positioned two antennas facing each other spaced by 240 mm and calculated the amplitude and phase of S21 and the group delay of the antenna. As shown in Fig.9 the variation of the group delay in this interval is lower than 0.4ns. Additionally, the amplitude of S21 remains approximately constant, and the phase of S21 is linear in the frequency range. Furthermore, side-by-side and face-to-face configuration scenarios were investigated and compared. As depicted in Fig.8, the group delay remains constant from 3 to 14 GHz in the side-by-side scenario, while the phase of S21 exhibits distortion specifically at the frequency of 14 GHz. Additionally, the amplitude of S21 experiences a decrease at this frequency.

To assess the performance of the antenna, two distinct signals are utilized as inputs. The first signal is a default Gaussian pulse generated within the CST software, spanning the frequency range specified by the UWB standard, which is between 3.1 GHz and 10.6 GHz (Signal I). The second signal is a sine-modulated Gaussian pulse with specific parameters, including a central frequency (Fc) of 7 GHz and a pulse width (b) of 220 ps (Signal II) [8, 25]. Figure 10(b) provides a visual representation of the normalized input signals. Then, the fidelity factor for both the E-plane and H-plane, based on the angle, is calculated. In the far-field region of the transmitting antenna, a total of 19 virtual probes are strategically positioned in both planes. These probes are evenly spaced at 10-degree intervals, ranging from -90 to 90 degrees along a circular trajectory centered at the antenna's midpoint (Figure 10).

Figure 10 illustrates a high-fidelity factor achieved in the E-plane, ranging from 0.922 to 0.975 for signal I. Furthermore, a fidelity factor between 0.831 and 0.975 was obtained for signal I in the H-plane. The fidelity factor for signal II exhibited slightly better performance, as it ranged from 0.979 to 0.990 across angles from -80 to 80 degrees in both the H-plane and E-plane.

Figure 11 illustrates examples of the normalized radiated signals in both the E-plane and H-plane at various angles along the specified arcs. The signals depicted in Figure 11 demonstrate the antenna's capability to transmit short pulses with minimal signal distortion.

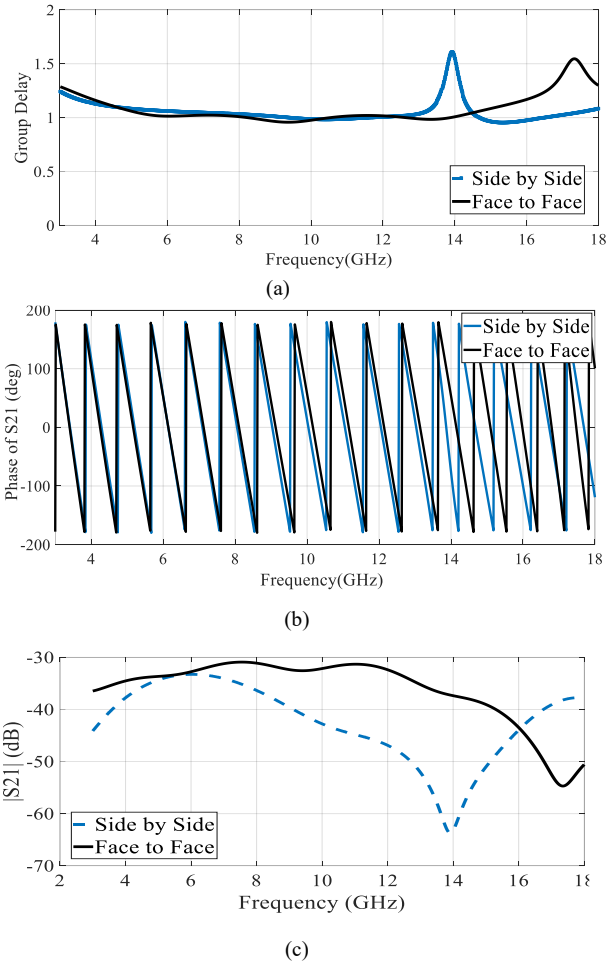

Fig. 9. (a) Group delay, (b) phase of S21, and (c) amplitude of S21 of the simulated antennas in the face-to-face and side-by-side scenario

VI Imaging Result

The system configuration for breast tumor detection is depicted in Figure 12. The primary goal is to detect changes in the backscattering signal in the presence or absence of a tumor with a high dielectric inclusion. The breast model used in this setup comprises two layers: the breast tissue layer and the skin layer. A tumor is situated 6 mm underneath the skin layer.

The performance evaluation of the proposed system involved examining the S21 parameter for different configurations: free space, the breast model with a tumor, and the breast model without a tumor. To obtain the S-parameters, two antennas were positioned in a face-to-face configuration around the breast model, maintaining a separation distance of 12 mm from the skin layer. Also, the S11 parameter was derived by positioning the antenna in front of the breast model. It was

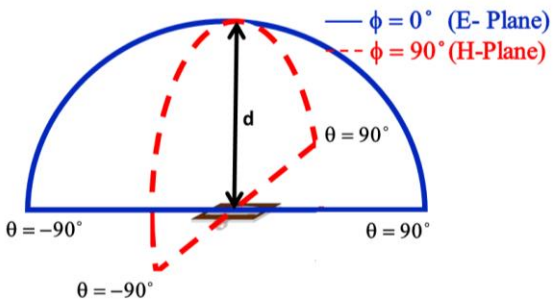

(a)

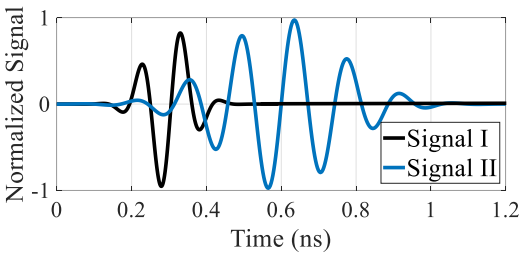

(b)

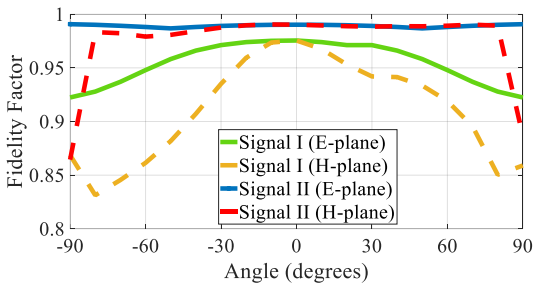

(c)

Fig. 10. (a) The far-field radiation performance evaluation of the antenna along arcs with a radius of 240 mm, (b) the waveform of input signals, and (c) the calculated fidelity factor of the wide-slot antenna, in the E-plane and H-plane.

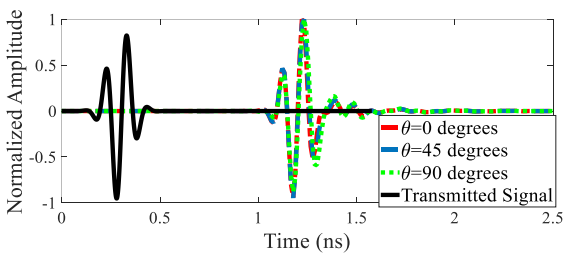

(a)

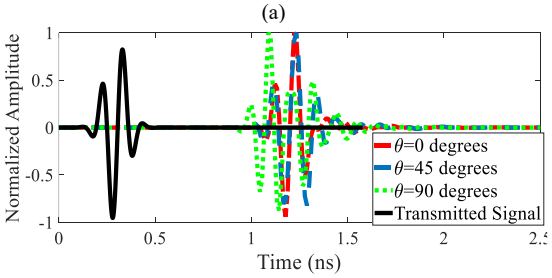

(b)

Fig. 11. Examples of the normalized radiated signals at (a) E-plane and (b) H-plane.

TABLE 2 FIDELITY FACTOR COMPARISON OF THE UWB ANTENNA WITH OTHER LITERATURE

Ref.	Bandwidth	Dimensions(mm)^3	Fidelity Factor	
[25]	3.5-11	39×36.6 (Signal II)	(Phi=0°, Theta=0°)= 0.9131 (Phi=0°, Theta=90°)=0.9002	
[26]	1.6-7.1	51.6×51.6 (Sine-Gaussian)	0.65-0.95	
[27]	2.8-11.5	29×24 (Signal I)	**E-plane** FtF=0.9091 SbS=0.8283	**H-plane** SbS=0.8270
[28]	4-11	20×19 (Signal I)	**E-plane** FtF=0.906 SbS=0.8524	
[32]	3.8-10.1	29×26.6 (Signal I)	**E-plane** FtF=0.916 SbS=0.912	
[34]	3.02-12	29.2×32.2 (Gaussian)	**E-plane** FtF=0.8633 SbS=0.9486	
Our work	3 -13	16×20 (Signal I) (Signal II)	**E-plane** 0.922 - 0.975 0.986 - 0.990	**H-plane** 0.831-0.975 0.864-0.990

Table 3 presents detailed information about the properties of the breast components at a frequency of 3 GHz [20, 28].

TABLE 3 GEOMETRICAL PARAMETERS AND ELECTRICAL PROPERTIES OF THE BREAST MODEL

Tissue	Conductivity (S/m)	Permittivity	Thickness (mm)
Skin	1.8	38	2.5
Tumor	3.1	67	10
Fat	0.1	5	87.5

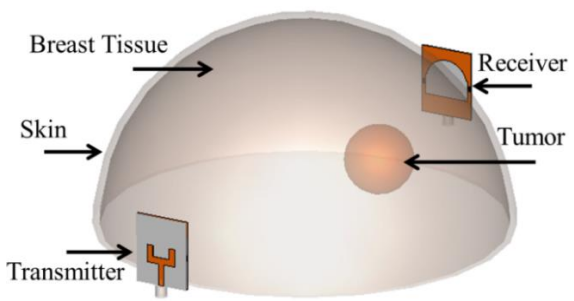

Fig. 12. Breast phantom model and simulation setup for microwave imaging

found that minimal variations were detected when compared to the configuration where the antenna was situated in free space.

The initial section of Figure 13 effectively showcases the strong performance of S11 when measured in front of the breast model. It demonstrates a noticeable difference in S21 between the scenarios with and without a tumor in the breast model. This contrast highlights the impact of tumors on the transmission characteristics. Furthermore, a significant variation in the transmission parameter can be observed across

the entire frequency range, the scenarios with and without the presence of the tumor.

Figures 14 and 15 present the assessment of Power Loss Density (PLD) and Specific Absorption Rate (SAR) for tissues with and without a tumor at 9.1 GHz. In healthy tissues, a uniform distribution of electrical energy is observed. However, the presence of a tumor disrupts this uniformity, leading to variations in the power distribution. The tumor absorbs some energy, resulting in deflections and changes in the power distribution pattern. The color density is noticeably higher in cancerous breasts than in healthy breasts. This difference in color density is attributed to the diverse dielectric properties present within the breast phantom models. These findings demonstrate the impact of tumors on the power distribution and highlight the variations in PLD between healthy and cancerous tissues. Also, we investigated the SAR for a sample weighing 0.01 g at a frequency of 9.1 GHz. This choice of sample size allows for quicker calculation of the SAR results. For both a healthy breast and a breast with a tumor, a maximum SAR of 5.56 W/kg was considered.

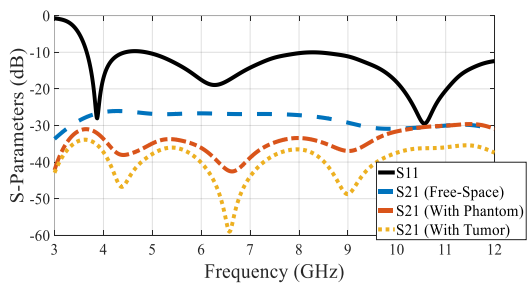

Fig. 13. S-parameters of the imaging setup

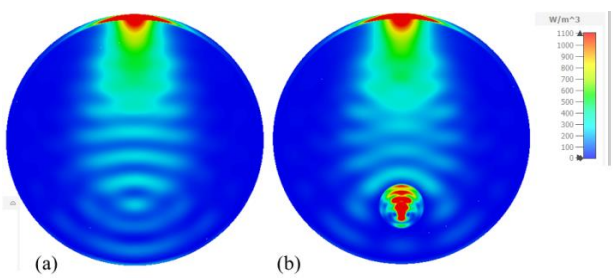

Fig. 14. Power loss density for normal and cancerous Breast

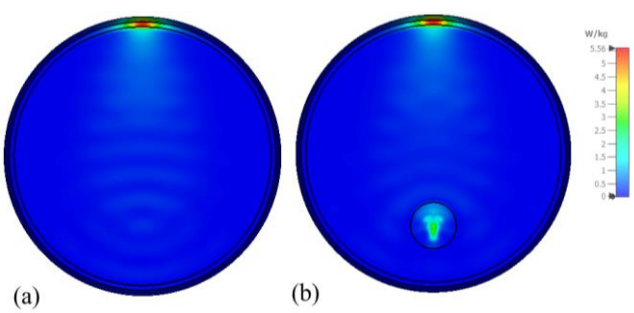

Fig. 15. Specific absorption rate for normal and cancerous Breast

VII Comparison

The fidelity (correlation) factor of antennas is an important criterion for tumor detection in microwave imaging applications. Table 2 compares the fidelity factor of the new design, and some structures addressed in recent literature on microwave imaging. As can be seen, the antenna in this project demonstrates reliable performance in terms of the fidelity factor at all angles compared to the most recent works.

Also, the innovative UWB antenna proposed in this study is compared to previously published UWB antennas for tumor detection, as presented in Table 4. Compared to previously published UWB antennas for Microwave Imaging, the proposed UWB antenna showcases notable features: its compact size and wide frequency range, as demonstrated by the comparative table. This smaller form factor contributes to its uniqueness and sets it apart from the previously mentioned antennas. The proposed antenna, despite its small size and without the use of a reflector or additional structural elements, offers an acceptable gain compared to other antennas.

TABLE 4 COMPARISON OF THE PROPOSED UWB ANTENNA WITH OTHER LITERATURE

Ref.	Dimensions(λ)^3	Operational Range[GHz]	Bandwidth (%)	Gain (dB))	Application
[29]	0.23×0.27×0.016	3.1-16	135	5	Microwave Imaging
[30]	0.4×0.4×0.0.015	2.79-8.93	104.8	4.03	Microwave Imaging
[31]	0.32×0.3×0.018	3.58-14	119	4.7	Energy harvesting
[32]	0.37×0.34×0.02	3.8-10.1	90.6	6.8	Microwave Imaging
[33]	0.24×0.20×0.015	2.79-18	146	5.74	Microwave Imaging
[34]	0.29×0.32×0.25	3.02-12	119	7.3	Microwave Imaging
[35]	0.33×0.33×0.09	2-5	85	8.47	Microwave Imaging
Pro.	0.20×0.25×0.012	3.7-18	131	6.3	Microwave Imaging

VIII Conclusions

The performance characteristics of an antenna were analyzed, studied, and optimized using the 3D simulator CST Microwave Studio 2018. Additionally, the proposed antenna was experimentally verified, demonstrating a satisfactory agreement between the simulation and measurement results. The fidelity factor was examined for both E-plane and H-plane scenarios, indicating a good range of 0.922 - 0.975 for the E-plane across all angles. With its smaller size, simple design, less signal distortion, and commendable performance, the proposed antenna is an excellent choice for implementing breast tumor imaging applications. Finally, a simulation model was suggested including a breast phantom with a tumor, along with transceiver. The performance of the antennas on the breast phantom was validated by studying parameters such as isolation and SAR. The proposed UWB antenna exhibited excellent characteristics, including a high gain of 6.3 dBi and

a fractional bandwidth percentage of 131%. Moreover, it achieved a remarkable efficiency of over 93.7% at the operational frequency of 6 GHz within the specified range. The antenna's fidelity factor was evaluated to assess distortion level in various scenarios. The maximum fidelity factor of 0.975 was achieved for the E-plane.

To show the effectiveness of using the new antenna, an MI simulation for breast tumor detection was performed to detect changes in the backscattering signal in the presence or absence of a tumor with a high dielectric inclusion. It was shown that S11 was quite high when measured in front of the breast model. Additionally, there was a noticeable difference in S21 between the scenarios with and without a tumor in the breast model. This contrast highlights the impact of tumors on the transmission characteristics. Furthermore, a significant variation was observed in the transmission parameter across the entire frequency range, the scenarios with and without the presence of the tumor.

ACKNOWLEDGMENTS

The authors would like to thank the Antenna Laboratory of K. N. Toosi University of Technology for measuring the antenna parameters.

REFERENCES

[1] E. C. Fear, S. C. Hagness, P. M. Meaney, M. Okoniewski, and M. A. Stuchly, "Enhancing breast tumor detection with near-field imaging," *IEEE Microwave magazine,* vol. 3, no. 1, pp. 48-56, 2002.

[2] Kahar, A. Ray, D. Sarkar, and P. Sarkar, "An UWB microstrip monopole antenna for breast tumor detection," *Microwave and Optical Technology Letters,* vol. 57, no. 1, pp. 49-54, 2015.

[3] M. Z. Mahmud, M. T. Islam, N. Misran, S. Kibria, and M. Samsuzzaman, "Microwave imaging for breast tumor detection using uniplanar AMC based CPW-fed microstrip antenna," *IEEE Access,* vol. 6, pp. 44763-44775, 2018.

[4] V. De Santis, J. M. Sill, J. Bourqui, and E. C. Fear, "Safety assessment of ultra-wideband antennas for microwave breast imaging," *Bioelectromagnetics,* vol. 33, no. 3, pp. 215-225, 2012.

[5] U. Rafique, S. Pisa, R. Cicchetti, O. Testa, and M. Cavagnaro, "Ultra-Wideband Antennas for Biomedical Imaging Applications: A Survey," *Sensors,* vol. 22, no. 9, p. 3230, 2022.

[6] M. Jalilvand, X. Li, L. Zwirello, and T. Zwick, "Ultra wideband compact near-field imaging system for breast cancer detection," *IET Microwaves, Antennas & Propagation,* vol. 9, no. 10, pp. 1009-1014, 2015.

[7] S. M. Aguilar, M. A. Al-Joumayly, M. J. Burfeindt, N. Behdad, and S. C. Hagness, "Multiband miniaturized patch antennas for a compact, shielded microwave breast imaging array," *IEEE transactions on antennas and propagation,* vol. 62, no. 3, pp. 1221-1231, 2013.

[8] Z. Lasemi and Z. Atlasbaf, "Impact of fidelity factor on breast cancer detection," *IEEE Antennas and Wireless Propagation Letters,* vol. 19, no. 10, pp. 1649-1653, 2020.

[9] F.-E. Zerrad *et al.*, "Multilayered metamaterials array antenna based on artificial magnetic conductor's structure for the application diagnostic breast cancer detection with microwave imaging," *Medical Engineering & Physic,* vol. 99, p. 103737, 2022.

[10] G. Quintero, J.-F. Zurcher, and A. K. Skrivervik, "System fidelity factor: A new method for comparing UWB antennas," *IEEE Transactions on Antennas and Propagation,* vol. 59, no. 7, pp. 2502-2512, 2011.

[11] R. Cicchetti, V. Cicchetti, A. Faraone, L. Foged, and O. Testa, "A compact high-gain wideband lens Vivaldi antenna for wireless communications and through-the-wall imaging," *IEEE transactions on antennas and propagation,* vol. 69, no. 6, pp. 3177-3192, 2020.

[12] N. Sharma and S. S. Bhatia, "Performance enhancement of hexagonal ring-shaped compact multiband integrated wideband fractal antennas for wireless applications," *International Journal of RF and Microwave Computer-Aided Engineering,* vol. 30, no. 3, p. e22079, 2020.

[13] S. Guruswamy, R. Chinniah, and K. Thangavelu, "A printed compact UWB Vivaldi antenna with hemi cylindrical slots and directors for microwave imaging applications. AEU—Int," *J. Electron. Commun,* vol. 110, p. 152870, 2019.

[14] C. Zhao, X. Li, M. Yang, and C. Sun, "Resistance-loaded miniaturized dual-layer Vivaldi antenna for plasma reflection diagnosis," *Microwave and Optical Technology Letters,* vol. 63, no. 1, pp. 205-210, 2021.

[15] N. Nurhayati, A. M. De Oliveira, J. F. Justo, E. Setijadi, B. E. Sukoco, and E. Endryansyah, "Palm tree coplanar Vivaldi antenna for near field radar application," *Microwave and Optical Technology Letters,* vol. 62, no. 2, pp. 964-974, 2020.

[16] M. Yousefnia, A. Ebrahimzadeh, M. Dehmollaian, and A. Madannejad, "A time-reversal imaging system for breast screening: Theory and initial phantom results," *IEEE Transactions on Biomedical Engineering,* vol. 65, no. 11, pp. 2542-2551, 2018.

[17] I. M. Danjuma, M. O. Akinsolu, C. H. See, R. A. Abd-Alhameed, and B. Liu, "Design and optimization of a slotted monopole antenna for ultra-wide band body centric imaging applications," *IEEE Journal of Electromagnetics, RF and Microwaves in Medicine and Biology,* vol. 4, no. 2, pp. 140-147, 2020.

[18] S. N. Mahmood *et al.*, "Full ground ultra-wideband wearable textile antenna for breast cancer and wireless body area network applications," *Micromachines,* vol. 12, no. 3, p. 322, 2021.

[19] Z. Lasemiimeni, Z. Atlasbaf, and N. Karbaschi, "Dual-functional ultrawideband antenna with high fidelity factor for body area networks and microwave imaging systems," *IEEE Access,* vol. 9, pp. 112930-112941, 2021.

[20] M. T. Islam, M. Samsuzzaman, M. Rahman, and M. Islam, "A compact slotted patch antenna for breast tumor detection," *Microwave and Optical Technology Letters,* vol. 60, no. 7, pp. 1600-1608, 2018.

[21] M. Mehranpour, S. Jarchi, A. Keshtkar, A. Ghorbani, A. Araghi, and M. Khalily, "Low-profile aperture stacked patch antenna for early-stage breast cancer detection applications," *International Journal of RF and Microwave Computer-Aided Engineering,* vol. 31, no. 3, p. e22531, 2021.

[22] M. T. Islam, M. Samsuzzaman, M. Faruque, M. J. Singh, and M. Islam, "Microwave imaging based breast tumor detection using compact wide slotted UWB patch antenna," *Optoelectron. Adv. Mater. Rapid Commun,* vol. 13, pp. 448-457, 2019.

[23] H. Bahramiabarghouei, E. Porter, A. Santorelli, B. Gosselin, M. Popović, and L. A. Rusch, "Flexible 16 antenna array for microwave breast cancer detection," *IEEE Transactions on Biomedical Engineering,* vol. 62, no. 10, pp. 2516-2525, 2015.
[24] D. Gibbins, M. Klemm, I. J. Craddock, J. A. Leendertz, A. Preece, and R. Benjamin, "A comparison of a wide-slot and a stacked patch antenna for the purpose of breast cancer detection," *IEEE transactions on antennas and propagation,* vol. 58, no. 3, pp. 665-674, 2009.
[25] B. Yeboah-Akowuah, P. Kosmas, and Y. Chen, "A Q-slot monopole for UWB body-centric wireless communications," *IEEE Transactions on Antennas and Propagation,* vol. 65, no. 10, pp. 5069-5075, 2017.
[26] A. Akbarpour, and S. Chamaani. "Ultrawideband circularly polarized antenna for near-field SAR imaging applications," *IEEE transactions on antennas and propagation ,* vol. 68, no. 6, pp. 4218-4228, 2020.
[27] A. Hossain, *et al*. "An octagonal ring-shaped parasitic resonator based compact ultrawideband antenna for microwave imaging applications," *Sensors* 20(5): 1354. vol. 20, no. 5, p. 1354, 2020.
[28] F.-E. Zerrad *et al.*, "Novel measurement technique to detect breast tumor based on the smallest form factor of UWB patch antenna," *International Journal of Microwave and Wireless Technologies,* vol. 15, no. 2, pp. 227-235, 2023.
[29] Z. Khan, A. Razzaq, J. Iqbal, A. Qamar, and M. Zubair, "Double circular ring compact antenna for ultra-wideband applications," *IET Microwaves, Antennas & Propagation,* vol. 12, no. 13, pp. 2094-2097, 2018.
[30] H. Jumaat, K. H. Ping, N. H. Abd Rahman, H. Yon, and F. N. M. Redzwan, "A compact modified wideband antenna with CBCPW, stubline and notch-staircase for breast cancer microwave imaging application," *AEU-International Journal of Electronics and Communications,* vol. 129, p. 153492, 2021.
[31] M. S. Jameel, Y. S. Mezaal, and D. C. Atilla, "Miniaturized coplanar waveguide-fed UWB Antenna for wireless applications," *Symmetry,* vol. 15, no. 3, p. 633, 2023.
[32] F.-e. Zerrad *et al.*, "Microwave Imaging Approach for Breast Cancer Detection Using a Tapered Slot Antenna Loaded with Parasitic Components," *Materials,* vol. 16, no. 4, p. 1496, 2023.
[33] H. T. Sediq, "Tumor detection concepts using eagle-shaped UWB antenna signals for medical purposes," *Sensors and Actuators A: Physical,* vol. 362, p. 114653, 2023.
[34] D.Awan, S. Bashir, S. Khan, S.S. Al-Bawri, and M. Dalarsson, "UWB Antenna with Enhanced Directivity for Applications in Microwave Medical Imaging," *Sensors*, vol. 24, no.4, p.1315, 2024.
[35] M.N. Hamza, S. Koziel, and A. Pietrenko-Dabrowska, "Design and experimental validation of a metamaterial-based sensor for microwave imaging in breast, lung, and brain cancer detection,".*Scientific Reports*, vol. 24, no.1, p.16177, 2024.
[36] F.Kazemi, "A Compact Antenna with Dual Polarization for Mobile and Wireless Communication," *International Journal of Industrial Electronics Control and Optimization*, vol. 6, no.1, pp.73-82. 2023.

MS Motahareh Arezoomandan is currently working toward the doctoral degree with the Faculty of Electrical and Electronics Engineering at the University of Sistan and Baluchestan, Zahedan, Iran. She received the M.Sc. degree in Telecommunication Engineering from the University of Semnan, Semnan, Iran, in 2014, and the B.Sc. degree in Electrical and Electronics Engineering from the University of Birjand, Birjand, Iran, in 2011. Her current research interests include microwave imaging, antenna propagation, and antenna design for mobile and wireless communication systems.

Dr. Shahram Mohanna received a Ph.D. degree in electronics engineering from the University of Manchester in July 2006 and a M.Sc. in Telecommunications Engineering from University of Shiraz, Iran. He worked as a research assistant in the Sensing, Imaging and Signal Processing (SISP) Research Centre at the University of Manchester from 2002 to 2006. During 2012 and 2016, he joined the University of Nottingham Malaysia (UNM) as an associate professor until September 2016 then moved to the University of Sistan and Baluchestan, Zahedan, Iran, as an associate professor. As a multidisciplinary researcher, skillful in microwave imaging, electromagnetic tomography, ultrasonic and wireless sensors, and related physics and mathematics, he has contributed to the discipline by delivering 18 articles in international conferences and publishing 31 papers in indexed journals.

Dr. Ahmad Bakhtiyari Shahri received the B.Sc. degree in electrical and electronic engineering from the University of Sistan and Baluchestan (USB), Zahedan, Iran, in 1999, and the M.Sc. degrees in Telecommunications Engineering in 2006 and a PhD degree in Computer Science from the University of Malaya, Malaysia in 2015. He is currently an assistant professor and director of Education Services in USB. He is expert in Internet of Things (IoT) and IoT security and delivered 8 articles to international conferences and has published 10 journals papers.